Development of a Novel Storm Surge Inundation Model Framework for Efficient Prediction

Xuanxuan Gao [1, 3], Shuiqing Li [1, 2, 3, 4], Dongxue Mo [1, 2, 3, 4], Yahao Liu [1, 2, 3, 4], and Po Hu [1, 2, 3, 4]

[1]Key Laboratory of Ocean Observation and Forecasting, Key Laboratory of Ocean Circulation and Waves, Institute of Oceanology, Chinese Academy of Sciences, Qingdao, 266071, China
[2]Laboratory for Ocean and Climate Dynamics, Pilot National Laboratory for Marine Science and Technology (Qingdao), Qingdao, 266237, China
[3]University of Chinese Academy of Sciences, Beijing, 100049, China
[4]Center for Ocean Mega-Science, Chinese Academy of Sciences, Qingdao, 266071, China

Correspondence to: Shuiqing Li (lishuiqing@qdio.ac.cn), Po Hu (hupo@qdio.ac.cn)

Abstract. Storm surge is a natural process that generates flood disasters in coastal zone and causes massive casualties and property losses. Therefore, the storm surge inundation is of major concern in formulating appropriate strategies for disaster prevention and mitigation. However, traditional storm surge hydrodynamic models have large limits on computational efficiency and stability in practical applications. In this study, a novel storm surge inundation model was developed based on a wetting and drying algorithm established from simplified shallow water momentum equation. The wetting and drying algorithm was applied to rectangle grid that iterates through cellular automata algorithm to improve computational efficiency. The model, referred to as the Hydrodynamical Cellular Automata Flood Model (HCA-FM), was evaluated by comparing the simulations to regional field observations and that from a widely used hydrodynamic numerical model, respectively. The comparisons demonstrated that HCA-FM can reproduce the observed inundation distributions, and predict consistent results with the numerical simulation in terms of the inundation extent and submerged depth, with much improved computational efficiency (predict inundation within a few minutes) and high stability. The results reflect significant advancement of HCA-FM toward efficient predictions of storm surge inundation and applications at large space scales.

1 Introduction

Storm surge, defined as the abnormal water rise (or fall) due to strong winds and/or air pressure gradients, usually tropical cyclones. This coastal water rise combined with the high tide and waves would cause massive inundation. According to the Bulletin of China Marine Disaster, storm surge is the major marine hazard in China, which can cause huge casualties and property damage. Considering the trend of sea level rise (Hauer et al., 2021) and land subsidence, the risk of storm surge inundation in coastal zones is increasingly prominent. Therefore, considerable attention has been given to building accurate and efficient models for the simulation of storm surge inundation, which involves the extent of inundation, submerged depth, and flow velocity whenever technically possible.

Hydrodynamic models that simulate storm surge by numerically solving shallow water equations on a grid (Teng et al., 2017) have been developed and widely used, such as the MIKE21 (e.g., Machineni et al., 2019), the Finite Volume Community Ocean Model (FVCOM) (e.g., Nakamura et al., 2019) and the Advanced Circulation (ADCIRC) model (e.g., Li et al., 2022). These models can also be coupled with nearshore wave models (e.g., Mao and Xia, 2017; Wang et al., 2021).

Aiming to model the storm surge inundation, wetting and drying algorithms have been applied to manage the state transition of elements between wet and dry. The existing algorithms differ in complexity which is related to the computational efficiency, stability and simulation accuracy (Medeiros & Hagen, 2013). The common thread of different algorithms is to design the judgment conditions for grid wetting and drying, which usually uses a criterion by setting a critical value on a physical quantity. The water depth is generally chosen as the physical quantity, with a minimum depth in the wetting and drying judgment (e.g., Luettich and Westerink, 1999). These numerical inundation model, such as ADCIRC (e.g., Wang et al., 2020; Shi et al., 2022) and FVCOM (e.g., Saswati Deb et al., 2021), has been used in several researches to successfully simulate storm surge inundation. These storm surge inundation models embed physics well and thus has high simulation accuracy. However, it is hard to balance scientific accuracy, numerical stability, and computational efficiency in computer modeling. To guarantee the spatial accuracy and computational stability of the storm surge inundation simulation, the grid resolution must be increased, and the time step must be reduced to ensure model stability, which significantly increases the computational cost. ~~numerical models have high computational cost and instability due to their numerical complexity and thus are not suitable for applications over large study areas.~~

Although some efforts have been made to enhance the efficiency (1 to 2 orders of magnitude) of hydrodynamic models through several approaches, such as, neglecting terms in shallow water equations to reduce complexity (e.g., Hunter et al., 2007; Bates et al., 2005; Bates et al., 2010), applying computing technique (e.g., Sanders et al., 2010; Kalyanapu et al., 2011; Vacondio et al., 2017; Roberts et al., 2021), applying subgrid theory (e.g., Volp et al., 2013; Sehili et al., 2014; Kennedy et al., 2019; Begmohammadi et al., 2021; Woodruff et al., 2021), it is still not efficient enough to meet the needs of emergency applications. And it is not convenient for practical use as many complicated preparations must be done before using a hydrodynamic model, particular for a unstructured mesh, including mesh generation, mesh quality adjustment, and input file generation. Thus, an accurate and efficient storm surge inundation model is urgently needed.

Distinguished from storm surge hydrodynamic models solving shallow water equations, several models for urban flood have been developed for rapid simulation, which could be collectively described as conceptual models. Conceptual models that are mostly used, such as digital elevation model (DEM) based (e.g., Jamali et al., 2018; Manfreda and Samela, 2019; Miura et al., 2021) and Cellular Automata (CA) based models (e.g., Jamali et al., 2019; Wijaya and Yang, 2020, 2021), are essentially designed for free surface floods. DEM-based models calculate the water distribution above the geographical environment based on the so-called theory the “bathtub method”, which assumes a planar water surface. CA-based models have been developed in recent years, and the water volume balance is the most common used basic theory to design the wetting and drying transition rules of CA. Compared with hydrodynamic models, conceptual models have a significant advantage in terms of high computational efficiency, which is crucial to practical applications requiring timeliness. However,

the water distribution in simplified conceptual models is mainly controlled by the force of gravity, which ignore dynamic forces that influence the flood process, such as wind stress and bottom friction, that is important for storm surge inundation. But the basic grid iteration method is worth learning and helps to achieve the design of efficient storm surge inundation model.

In this paper, we propose a novel storm surge inundation model that embeds fluid physics in wetting and drying algorithm and uses CA algorithm to improve computational efficiency. In Sect. 2, the development of the model framework is introduced. Sect. 3 presents model verification and validation against field observations and hydrodynamic model simulations for several typical storm surge inundation events to validate its accuracy by performing comparisons. Finally, in Sect. 4, we analyse the advantages of the model to illuminate its application perspective.

2 Model design

2.1 Wetting and drying algorithm

The wetting and drying algorithm is the basis of a flooding model (Medeiros & Hagen, 2013), which models spread of water on the computational grid by defining transition rules that govern the state transition of an element between wet and dry. In contrast to transition rules based on the water volume balance in the urban flood model, the transition rules in our model were dynamically designed based on the shallow water momentum equation.

The momentum equation of two-dimensional shallow water equations is given as:

$$\underset{(i)}{\frac{\partial v}{\partial t}} + \underset{(ii)}{v\frac{\partial v}{\partial x}} = \underset{(iii)}{-g\frac{\partial \eta}{\partial x}} + \underset{(iv)}{\frac{\tau_a-\tau_b}{\rho d}} \tag{1}$$

where v is the depth-averaged velocity (m/s) in the direction of x, η is the water stage (m), τ_a is the wind stress (N/m^2) in the direction of x, τ_b is the bottom friction (N/m^2) in the direction of x, ρ is the seawater density (kg/m^3), g is gravity (m/s^2) and d is the water depth (m).

In Eq. (1), (i) represents the local inertia term, (ii) represents the advective inertia term, (iii) represents the pressure differential term and (iv) represents the external force terms including wind stress and bottom friction.

Neglecting the local inertia term, Eq. (1) is transformed into Eq. (2), which shows the effect of external forces on changing the total energy level.

$$\frac{\partial}{\partial x}\left(\eta + \frac{v^2}{2g}\right) = \frac{\tau_a-\tau_b}{\rho g d} \tag{2}$$

Consider two adjacent cells ($Cell_{tar}$ and $Cell_{ner}$) where $Cell_{ner}$ is wet and $Cell_{tar}$ is dry (Fig. 1). Assume that water will flow from $Cell_{ner}$ to $Cell_{tar}$ which will turn wet. Then, under this null hypothesis Eq. (2) is discretized into Eq. (3) by applying finite differences to act as the linkage between these two cells. We assume that the Froude numbers in the two cells are approximately equal, as expressed in Eq. (4).

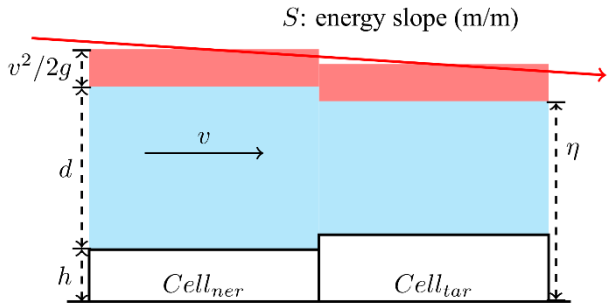

Figure 1: Illustration of hydrodynamic structure between the target cell and neighbor cell.

$$\frac{\left[\left(\frac{v_{tar}{}^2}{2g}+\eta_{tar}\right)-\left(\frac{v_{ner}{}^2}{2g}+\eta_{ner}\right)\right]}{\Delta x}=\frac{\tau_a-\tau_b}{\rho g d} \tag{3}$$

$$Fr=\frac{v_{tar}}{\sqrt{g(\eta_{tar}-h_{tar})}}=\frac{v_{ner}}{\sqrt{g(\eta_{ner}-h_{ner})}} \tag{4}$$

Thus, Eq. (5) is obtained by combining Eq. (3) and Eq. (4).

$$\eta_{tar}+\frac{Fr^2}{2}(\eta_{tar}-h_{tar})-\left(\eta_{ner}+\frac{V_{ner}{}^2}{2g}+\frac{\tau_a-\tau_b}{\rho g d}\Delta x\right)=0 \tag{5}$$

However, only if water level η_{tar} is higher than the ground elevation h_{tar}, is the null hypothesis that water flows from $Cell_{ner}$ to $Cell_{tar}$ made at the beginning true, i.e., that η_{tar} is greater than h_{tar}, becomes the condition for $Cell_{tar}$ to become wet. Furthermore, combined with Eq. (5), this condition can be transformed into Eq. (6), which describes the relationship between the elevation at $Cell_{tar}$ and the residual height of the energy line after wind forcing and bottom dissipation. Only when the elevation at a dry cell is less than the residual height of the energy line from its adjacent wet cell, will the dry cell be submerged.

$$h_{tar}<\eta_{ner}+\frac{V_{ner}{}^2}{2g}+\frac{\tau_a-\tau_b}{\rho g d}\Delta x \tag{6}$$

Thus, the water level in $Cell_{tar}$ is obtained by solving Eq. (5) and is expressed as Eq. (7). Then the flow velocity is also calculated as Eq. (8).

$$\eta_{tar}=\left(\eta_{ner}+\frac{V_{ner}{}^2}{2g}+\frac{\tau_a-\tau_b}{\rho g d}\Delta x+\frac{Fr^2}{2}h_{tar}\right)/\left(1+\frac{Fr^2}{2}\right) \tag{7}$$

$$v_{tar}=Fr\sqrt{g(\eta_{tar}-h_{tar})} \tag{8}$$

The wind stress and bottom friction are given as Eq. (9) and Eq. (11).

$$\tau_a=\rho_a C_d v_{wind}|v_{wind}| \tag{9}$$

$$C_d=\min[(0.75+0.067|v_{wind}|)\times 10^{-3},0.0035] \tag{10}$$

$$\tau_b=\rho C_f v|v| \tag{11}$$

$$C_f=\frac{gn^2}{d^{1/3}} \tag{12}$$

where τ_b is bottom friction, τ_a is wind stress, ρ is seawater density, ρ_a is air density, v_{wind} is the projection of relative wind in the direction of water flow, C_d is the drag coefficient suggested by Garratt (1977) with a high limit of 0.0035, C_f is the

bottom friction coefficient, and n is Manning's roughness coefficient, a parameter used to characterize the bed roughness that differs by land cover and can be determined according to the standard of American National Land Cover Data (NLCD) (Liu et al., 2019).

As bottom friction is reversed to flow, it will always reduce the energy level. The effect of wind force is determined by the relative direction between wind and current. Downstream wind will increase energy level while upstream wind has a similar effect as bottom friction.

2.2 Grid model

The wetting and drying algorithm describes the process of water flow from the wet cell to the adjacent dry cell, based on which the storm surge inundation model was built by applying Cellular Automata (CA) algorithm, a grid iteration method widely used in urban flood models.

CA is a mathematical idealized model that can simulate physical systems and processes (Wolfram, 1984). It is discrete spatiotemporally and consists of regular and rigid cells, each of which possesses a set of variables. As the values of variables at each cell are affected by its neighborhood and updated based on transition rules in discrete time steps, the CA evolves. The computational efficiency of the CA algorithm depends on the complexity of the transition rules. The flexibility of designing transition rules makes it possible to easily balance the simulation effect and computational efficiency.

In a flood map, the study area can be considered as a binary image, as the state at each position can only be wet or dry. Unlike rainfall-induced inundation, which has no boundary source, storm surge-induced inundation is caused by the abnormal rise of water along the coastline. As water flows according to the continuity of the fluid, the change in state of any position is only influenced by its neighborhoods within a delay time.

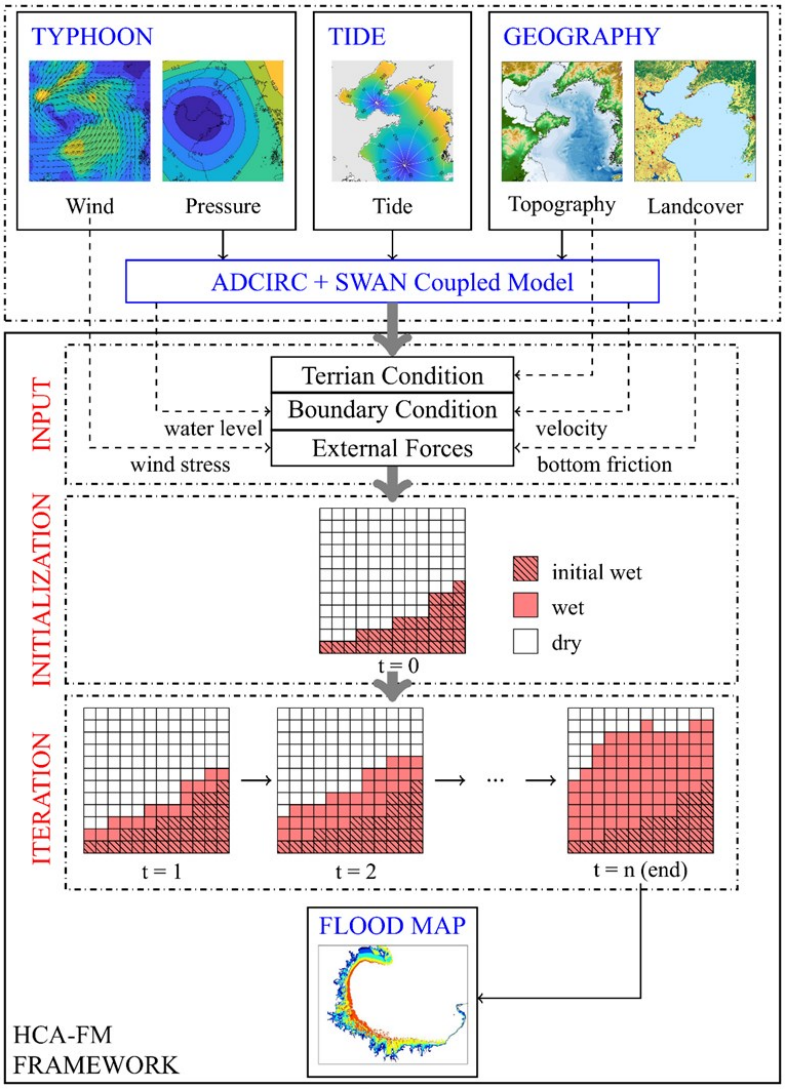

Figure 2: Framework of storm surge inundation simulation by HCA-FM.

Taking the wetting and drying algorithm as the transition rule of CA, a novel storm surge inundation model was built. A simulation by the HCA-FM includes the following steps and an instruction flowchart is also presented in Fig. 2:

(1) Input data preparation

In the HCA-FM, topography and land cover are used as constant geographic features in the study area. Land cover type will be transformed to Manning's coefficient according to NLCD to determine the bottom friction. The bottom friction together with wind stress are external forces which determine the energy slope between cells. Boundary conditions that include water level and flow velocity along coastline are used as triggers for storm surge inundation.

(2) Initialization

The study area is divided into rectangle cells with suitable resolution to maintain a good balance between spatial resolution and computational efficiency. The neighborhood is defined as the Moore neighborhood, which includes the cell itself, four cells with a common edge and four cells with a common vertex.

The ground elevation, Manning coefficient, and wind field are resampled to all cells while coastal water level and flow velocity are resampled to the initial wet cells. Cells with water levels larger than elevation are given the state of wetness expressed by 255 in the program while others are dry expressed by 0. Through these preparatory works, the initial cell structure of the HCA-FM is built.

(3) Grid iteration

Then each cell in the grid will iterate according to the wetting and drying algorithm introduced in Sect. 2.1. Briefly, in at least one of the eight directions, if the relationship between the target cell and wet neighbor cell satisfies Eq. (6), the target cell will turn wet. If more than one wet neighbor cell meets this criterion, the HCA-FM will regard them as one cell by averaging the residual energy height and Froude number. Then the submerged depth and flow velocity will be calculated by Eq. (7) and Eq. (8) respectively. These cells will be updated in the next iteration step, and others will remain. The same process will be performed for the whole grid step by step until no cell should be updated.

Following these three steps, the HCA-FM achieves simulation of storm surge inundation. The final inundation extent, level of submerged depth and flow velocity are obtained from the final set of wet cells, which describe the extent and degree of hazard.

3 Model assessment

3.1 Storms and area

The assessment of the HCA-FM was based on two aspects: validation against field observations and comparison with a numerical hydrodynamic model. Two typhoon storm surge cases were included in the experiments for each aspect.

In the validation against field observations, coastal zones of Cangzhou, Hebei and Shenzhen, Guangdong were selected as study regions and represent typhoon-induced storm surges that occurred in the Bohai Sea and the South China Sea, respectively. Typhoon Lekima (Fig. 3(a)) landed on Shandong Peninsula on October 11th, 2019, with a center maximum wind speed of grade 9 and increased severe storm surge in Bohai Bay and Laizhou Bay. The National Marine Environmental Forecasting Center organized teams to investigate disasters around the south coast of Bohai Bay. The approximate inundation extent in Cangzhou was obtained. Typhoon Hato (Fig. 3(b)) originated in the northwestern Pacific Ocean on August 20th, 2017. Due to its movement track and intensity, the Pearl River Delta region experienced strong winds and severe storm surges. The Marine Monitoring and Forecasting Center of Shenzhen organized teams to investigate disasters in key regions. The field survey data in Shenzhen after Typhoon Hato included several locations that underwent hard-hits, which could indirectly reflect the inundation extent. Due to the limitations of rough survey data, validation only relied on inundation extent.

In the validation against the numerical model, Laizhou Bay was selected as the study area, which is located south of Bohai and frequently experiences storm surges. Due to its unique geographic site and configuration, the magnitude of the surge level along the coastline of Laizhou Bay is higher than that along any other part of the Shandong Peninsula. As a result, coastal regions in Laizhou Bay are exposed to a more severe situation where enormous casualties and economic losses are more likely to occur. Lekima and Polly were two typhoon storm surge events that caused severe consequences around Laizhou Bay (Fig. 3(a)). Along the coastline of Laizhou Bay, Typhoon Lekima brought about a surge rise of approximately 150 to 200 cm, which loaded heavy risk on the coastal regions. Different from Lekima, of which the typhoon center passed directly through Laizhou Bay, Typhoon Polly passed through the south of Shandong Peninsula. Therefore, these two typhoon processes could represent different types of typhoon tracks to check the universality of the HCA-FM.

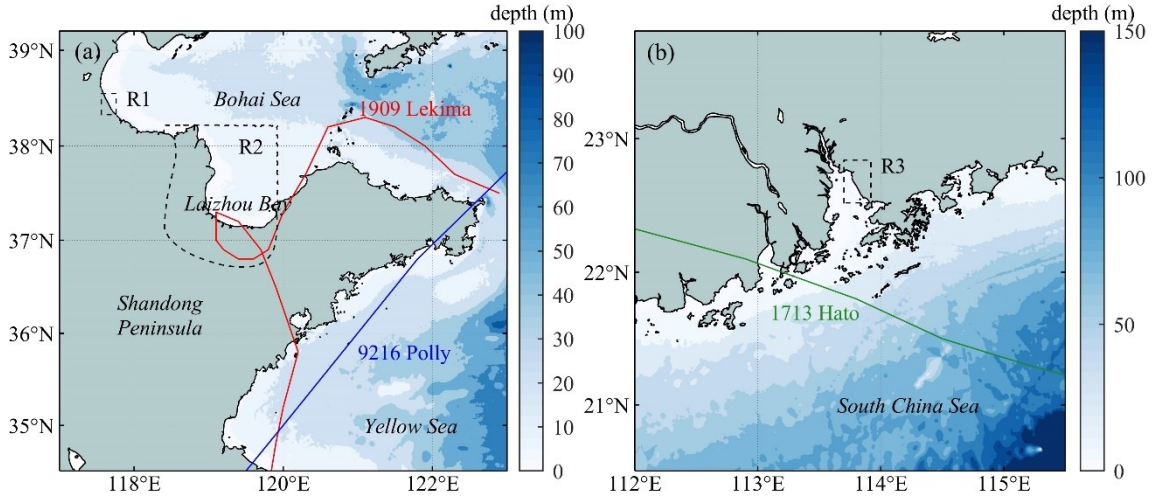

Figure 3: Typhoon tracks, bathymetry and study regions. (a) track of Lekima (1909) and Polly (9216); R1: Cangzhou, Hebei; R2: Laizhou Bay; (b) track of Hato (1713); R3: west coast of Shenzhen, Guangdong.

The HCA-FM was performed at Cangzhou during Lekima and the west coast of Shenzhen during Hato to validate the model simulations with field observations. Then, the HCA-FM and a hydrodynamic model called ADvanced CIRCulation + Simulating WAves Nearshore (ADCIRC+SWAN) coupled model were performed in the coastal region of Laizhou Bay during Lekima and Polly to make comparisons and validate the simulation accuracy of the HCA-FM. For the inundation simulation, the inundation extent and submerged depth are the aspects of greatest concern that determine the degree of ultimate consequence. Thus, these two aspects were chosen as indicators to measure the simulation consistency between the two models. ADCIRC+SWAN also provided boundary inputs, including the surge level and flow velocity, for the HCA-FM. Datasets that support ADCIRC+SWAN and HCA-FM model are available online and their sources are shown in Table 1.

Table 1: Sources of datasets that support ADCIRC+SWAN and HCA-FM model.

Name	Data sources
Bathymetric data	General Bathymetric Chart of the Oceans (GEBCO; https://www.gebco.net/)
Topographic data	ASTER GDEM v2 (The data set is provided by Geospatial Data Cloud site, Computer Network Information Center, Chinese Academy of Sciences; http://www.gscloud.cn)
Wind and pressure field	CFSR (from 1979 to 2010, Saha et al., 2010; https://rda.ucar.edu/datasets/ds093.1/) data from NECP CFSv2 (from 2010 to now, Saha et al., 2011; https://rda.ucar.edu/datasets/ds094.1/) data from NECP
Land cover	GlobeLand30 from National Geomatics Center of China (Chen et al, 2014; https://www.ngcc.cn/)
Typhoon tracks	China meteorological administration (Ying et al., 2014; Lu et al., 2021; http://tcdata.typhoon.org.cn)

3.2 Comparison with field observations

In the comparison of HCA-FM simulations with field observations, the visual image comparisons were made for the line or polygon features of inundation extent. Based on the field observations in Cangzhou after Typhoon Lekima and Shenzhen after Typhoon Hato, the HCA-FM was performed for these two cases. The boundary surge level and flow velocity were set as the temporal maximum conditions during storm surge processes. The inundation extents simulated by the HCA-FM and survey extents are presented in Fig. 4 and Fig. 5. It is important to note that due to the limitations of rough survey data, validation was based solely on inundation extent.

Figure 4: Comparison of inundation between the HCA-FM simulation and field observation in Cangzhou, Hebei during Typhoon Lekima; yellow line represents submerged boundary line simulated by the HCA-FM and blue line by field survey (Base map by Esri, Maxar, Earthstar Geographics, and the GIS User Community).

As shown in Fig. 4, the submerged boundary line simulated by the HCA-FM is basically consistent with field observations. The coastal region of Cangzhou is characterized by gentle terrain, waterways, and human-made seawalls. Most segments of the submerged boundary line are determined by seawalls because of the low-laying terrain. The flection of the submerged boundary line landwards is located near rivers, through which storm surge water rise spreads toward land more easily and causes further inundation compared with other regions. In other words, the HCA-FM can reflect the natural topography and human-made projects which enables simulation under a real geographical environment.

Figure 5 displays the comparison of the inundation extent between the simulation and field observations on the west coast of Shenzhen during Typhoon Hato. Overall, Hato brought heavy disasters to the west coast of Shenzhen. Seawater intruded landward for several kilometers due mainly to low-lying elevation and water intrusion backward through waterways. The detailed comparisons of three survey positions are presented as three subplots of Fig. 5.

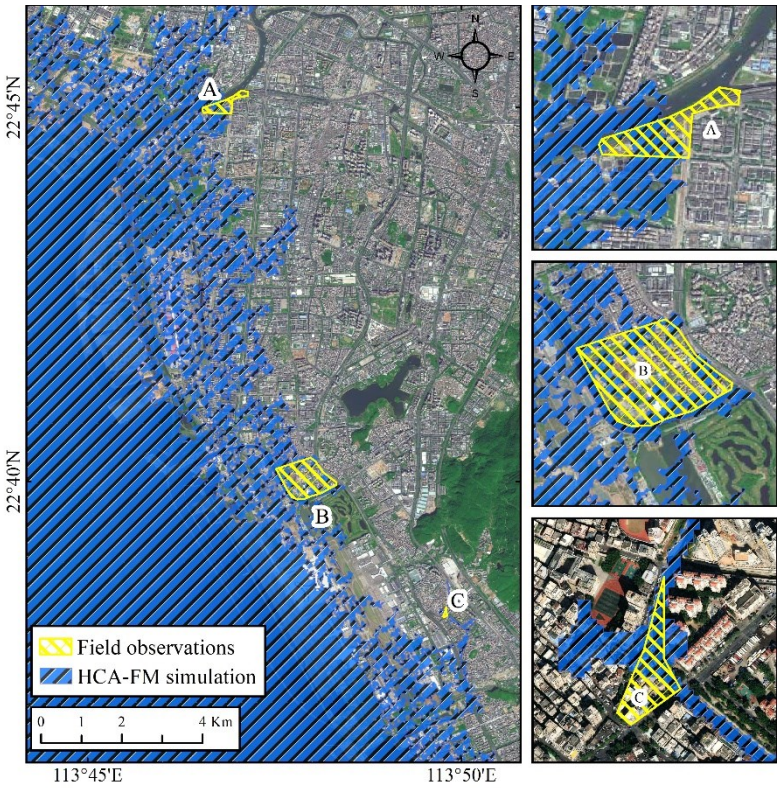

Figure 5: Comparison of inundation in three survey sites (A, B, C) on the west coast of Shenzhen, Guangdong during Typhoon Hato; blue region represents flood extent simulated by the HCA-FM and yellow polygons represent survey regions being submerged (Base map by Esri, Maxar, Earthstar Geographics, and the GIS User Community).

Considering the errors between the digital terrain model (DEM) and real terrain, the differences between HCA-FM simulation and survey data are acceptable. In additional, rainfall, which is not considered in the current HCA-FM, is another influencing factor that is blamed for generating the differences. The accuracy of the HCA-FM was validated. Moreover, these two comparison cases located on the coast of the Bohai Sea and the South China Sea also indicated the universality of the HCA-FM.

3.3 Comparison with Hydrodynamic Model

The numerical hydrodynamic model can represent the basic fluid mechanics well and thus is used here to assess the physical consideration of the HCA-FM. In reality, seawalls are built in coastal regions to prevent surge inundation. In this section, to focus on the inundation process, seawalls were neglected. This comparison experiment focused on the region around Laizhou Bay, during two storm surge events forced by Typhoons Lekima and Polly, respectively.

The numerical hydrodynamic model was chosen as the widely used the ADCIRC+SWAN coupled model. The ADCIRC model was developed by Luettich et al. (1992) and Westerink et al. (1994), and SWAN model was the third-generation wave model developed by Delft University of Technology (Booij et al., 1999). The ADCIRC+SWAN model couples the ADCIRC

and SWAN models by swapping data in the same grid and is generally applied for the simulation of tropical cyclone-induced storm surge and coastal inundation (Dietrich et al., 2011). The grid resolution of ADCIRC+SWAN model used in the comparison experiments ranges from 100 m on the inland coast to 20 km along the abyssal open boundary. The surge simulation ability of ADCIRC+SWAN model was well verified by tide station data (Li et al., 2023).

The input data of the maximum surge level and flow velocity at the initial wet cells in the HCA-FM were extracted from the ADCIRC+SWAN model to unify the boundary conditions. In addition to boundary conditions, bottom friction parameterizations can also influence model's performance (Chen et al., 2013). Considering that the bottom friction coefficient is defined as Eq. (13) in the ADCIRC+SWAN model, while defined as Eq. (12) in HCA-FM in the form of Manning's coefficient, it is necessary to use an equivalent bottom friction model in the experiments.

$$C_f = C_{f_{min}}\left[1 + \left(\frac{H_{break}}{d}\right)^{\theta}\right]^{\frac{\gamma}{\theta}} \tag{13}$$

where C_f is the bottom friction coefficient, $C_{f_{min}}$ is the minimum bottom friction coefficient, H_{break} is the break depth, d is the water depth, θ is a dimensionless parameter that defines how rapidly the bottom friction coefficient approaches its upper and lower limits, and γ is a dimensionless parameter that describes how quickly the bottom friction coefficient increases as the water depth decreases. $C_{f_{min}}$, H_{break}, θ, and γ are set as 0.0015, 1, 10 and 1/3, respectively, in the ADCIRC+SWAN model.

Based on the relationship between C_f and n in Eq. (12), an equivalent Manning's coefficient, as expressed in Eq. (14), was used in HCA-FM, which is related to water depth instead of land cover type.

$$n = \sqrt{\frac{0.0015 d^{\frac{1}{3}}}{g}\left[1 + \left(\frac{1}{d}\right)^{10}\right]^{\frac{1}{30}}} \tag{14}$$

Then, the extent and submerged depth of inundation during Typhoons Lekima and Polly around Laizhou Bay were simulated by the HCA-FM and ADCIRC+SWAN models respectively. Considering that different grid structure were used in these two models (orthogonal grids in HCA-FM while unstructured triangular grids in ADCIRC+SWAN model) and the grid resolution of HCA-FM was higher than the ADCIRC+SWAN model, the water depth simulated by HCA-FM was interpolated to the grid nodes of ADCIRC+SWAN model by bilinear interpolation to display water depth comparisons.

As a result, the comparison analysis of inundation results by the two models consisted of the following two aspects:

(1) A comparison of inundation extent was performed to demonstrate the accuracy of the simulated inundation range. The statistic used to assess the degree of consistency between the two models' simulated inundation extent was defined as the fit ratio δ (Horritt and Bates, 2001). δ ranges from 0 for no overlap to 1 for perfect fit.

$$\delta = \frac{N_o}{N_a + N_m - N_o} \tag{15}$$

where N_a is the number of wet points in the HCA-FM, N_m is the number of wet points in the ADCIRC+SWAN model, and N_o is the number of overlapping wet points.

(2) A comparison of the submerged depth at the overlapping wet points was performed to demonstrate the accuracy of the simulated submerged depth. Statistics to assess the consistency of the two groups of submerged depths simulated by the two models included R square (R^2) and root-mean-square errors (RMSE).

$$R^2 = \left[\frac{\sum_{i=1}^{N_o}(d_a^i-\overline{d_a})(d_m^i-\overline{d_m})}{\sqrt{\sum_{i=1}^{N_o}(d_a^i-\overline{d_a})^2\cdot\sum_{i=1}^{N_o}(d_m^i-\overline{d_m})^2}}\right]^2 \tag{16}$$

$$RMSE = \sqrt{\frac{1}{N_o}\sum_{i=1}^{N_o}[d_a^i - d_m^i]^2} \tag{17}$$

where d_a^i is the water depth at point i simulated by the HCA-FM, and d_m^i is the water depth at point i simulated by the ADCIRC+SWAN model.

Figure 6 shows the comparisons of simulated inundation between the HCA-FM and ADCIRC+SWAN models during Typhoons Lekima and Polly. Figure 6(a) and 6(c) displays the maximum inundation extent during Lekima and Polly by the two models. The green region is regarded to be submerged by both models, while the yellow and blue regions represent the overestimated and underestimated inundation areas, respectively, simulated by the HCA-FM compared with the ADCIRC+SWAN model. It was intuitively plausible that the HCA-FM simulated a basically consistent inundation extent with the ADCIRC+SWAN model. The fit ratio was 0.92 for Lekima and 0.95 for Polly, which was in accordance with intuition. Figure 6(b) and 6(d) displays the comparison of the submerged depth point-to-point simulated by the two models within the overlapping area during Lekima and Polly. Most of the dots are distributed around $y = x$ within an error of 0.3 m, the values of R^2 was 0.96 and $RMSE$ was 0.13 m for Lekima (R^2 was 0.96 and $RMSE$ was 0.12 m for Polly), indicated a good consistency between the HCA-FM and ADCIRC+SWAN models.

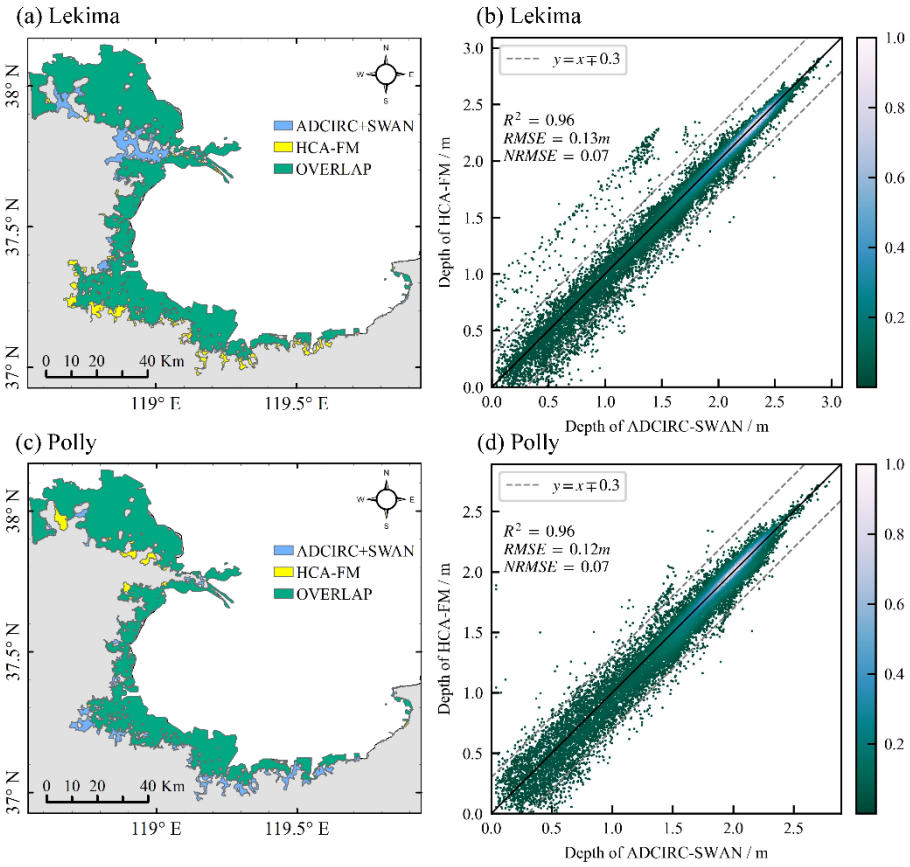

Figure 6: Comparison between the HCA-FM and ADCIRC+SWAN models. (a) & (c) Comparison of flood extent during Typhoons Lekima and Polly, respectively; (b) & (d) scatter plot of ADCIRC+SWAN versus HCA-FM simulated water depth during Lekima and Polly, respectively.

4 Discussions

Inundation models aim to serve realistic hazard management. Thus, it is necessary for them to provide flood maps that are sufficiently accurate. Image comparisons on inundation extent polygons were applied, and model simulations can reflect the real inundation for both storm surge events. Such results show the simulation accuracy of the HCA-FM under a real geographical environment, where seawalls and rivers are considered. On the other hand, image and indicator comparisons were applied to validate the model's accuracy and theoretical rationality in contrast to the ADCIRC+SWAN coupled model. With the fit ratio δ higher than 0.90, R^2 higher than 0.95 and $RMSE$ less than 0.15 m, a conclusion could be made that the error of the simulated inundation extent and submerged depth compared with the ADCIRC+SWAN model is basically small and acceptable. This acceptable error is relative to the grid structure difference (Tsubaki and Kawahara, 2013), model's simplified hydrodynamic basis, and simplifications on boundary conditions (Parizi et al., 2022).

The innovation of HCA-FM compared to conventional CA models is its hydrodynamic consideration of both wind force and bottom friction. Storm surge inundation differs from urban flooding in terms of the geographical and meteorological environment. The CA models for urban flooding mainly simulate the spreading of fluids to lower elevation areas under gravity, whereas storm surge inundation usually occurs in coastal areas, where seawater spreads not only to lower elevation areas under gravity, but also to higher elevation areas under dynamic forcing. In view of this, it is not appropriate to use the common CA models to simulate storm surge inundation.

Therefore, in order to illustrate the benefit of such considerations on the accuracy of the simulation, sensitivity experiments related to wind force and bottom friction were designed for two storm surge events.

Table 2 shows the consistency indicators of the four groups of sensitivity experiments. Experiment (Exp.) 1 represents the standard HCA-FM with consideration of both wind force and bottom friction, which provides the good simulation discussed above. Experiment 2 represents the model without consideration of wind force and bottom friction as many conceptual models do and provides a worse simulation with the R^2 less than 0.90 and $RMSE$ higher than 0.25 m. This comparison between Exp. 1 and Exp. 2 demonstrates the necessity of considering forces affecting water bodies. Experiment 3 and Exp. 4 represent experiments in which only wind force or bottom friction is considered, and both provide worse results compared with Exp. 1, among which Exp. 4, which considers bottom friction but ignores wind force, provides an even worse simulation. This finding shows that consideration of external forces improves the model's accuracy (Akbar et al., 2017; Chu et al., 2019) and that wind force plays a more dominant role than bottom friction in water propagation due to its important work in forcing seawater spreading.

Table 2: Consistency of simulated inundation around Laizhou Bay between the HCA-FM and ADCIRC+SWAN models in sensitivity experiments against wind force and bottom friction.

		Exp. 1	Exp. 2	Exp. 3	Exp. 4
Wind force		on	off	on	off
Bottom friction		on	off	off	on
Lekima (1909)	δ	0.92	0.89	0.91	0.84
	R^2	0.96	0.89	0.93	0.75
	$RMSE$ (m)	0.13	0.27	0.26	0.44
Polly (9216)	δ	0.95	0.91	0.91	0.87
	R^2	0.96	0.83	0.92	0.66
	$RMSE$ (m)	0.12	0.28	0.24	0.45

Note. **Here δ, R^2, and $RMSE$ represents the difference between HCA-FM and ADCIRC+SWAN simulations, the fit ratio of inundation range, R square and root-mean-square error of inundation depth, respectively.**

In addition, to illustrate the effects of wind stress and bottom friction on inundation in detail, a simplified typical terrain for storm surge inundation was designed with a constant slope (1:500), with the left side on the shore side and the right side on the sea side (Fig. 7). The inundation source is located at the position where the ground elevation is 0, with a constant water

level of 2.5 m and a constant onshore flow velocity of 1 m/s. For the onshore winds and bottom friction coefficient, we set up three sets of constant wind speeds of 0, 20, and 40 m/s (where the wind speed of 0 m/s corresponds to the common CA-flood models), and three sets of Manning's coefficient of 0.04, 0.06, and 0.08. According to the combination of the three sets of wind speeds and Manning's coefficient, the inundation simulations were carried out using the HCA-FM model.

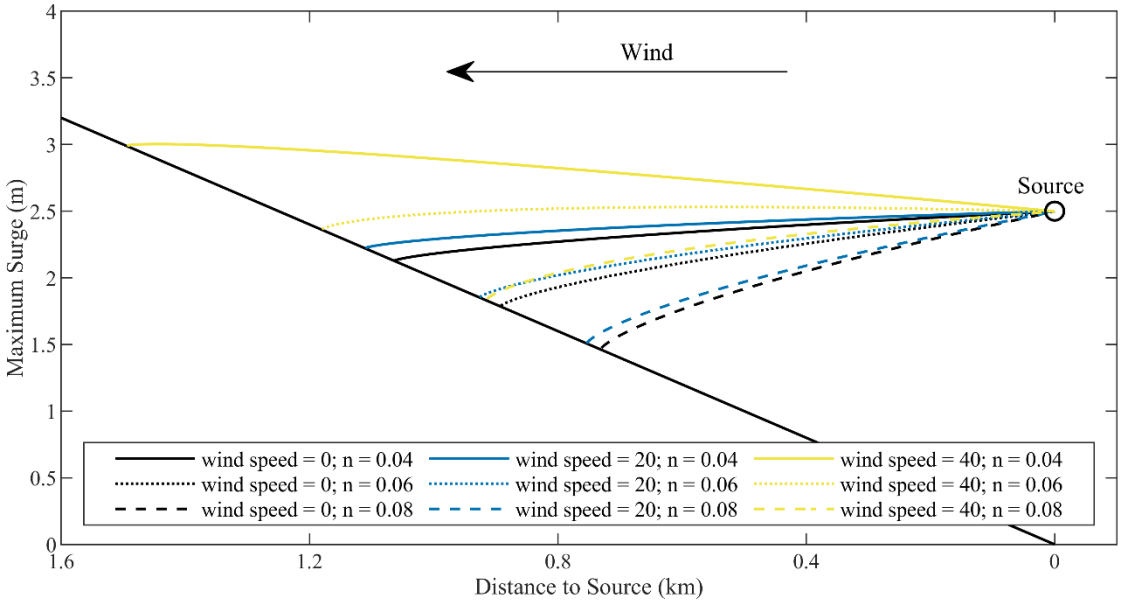

Figure 7: Maximum water level distribution under different wind speed and Manning's coefficient conditions.

Figure 7 shows the maximum water level distribution under different conditions of wind speed and Manning's coefficient. The bottom friction prevents the seawater from propagating to the shore, and under the same wind speed condition, the larger the Manning's coefficient (the larger the bottom friction coefficient), the smaller the inundation area and the smaller the inundation depth; the onshore wind forces the seawater to propagate to the shore, and under the same bottom friction condition, the larger the wind speed, the larger the inundation area and the larger the inundation depth. It can be seen that the wind plays an important role in the storm surge inundation process, and if the effect of onshore wind is not considered in the inundation simulation, the potential inundation area and water depth will be underestimated. Thus, it is shown that it is necessary to consider wind stress and bottom friction in storm surge inundation modelling, which is the advantage of the HCA-FM model over the common CA flooding models.

These comparisons and sensitivity experiments result in the conclusion that the HCA-FM provides simulation consistent with the ADCIRC+SWAN model and is superior to most existing conceptual urban flood models. In addition to the accuracy of the HCA-FM, this simulation method's advantage also lies in its computational efficiency due to the simplified wetting and drying algorithm (transition rules) derived from the shallow water equations. ~~use of a CA algorithm compared with a numerical model.~~ In comparison, traditional methods like numerical model solve hydrodynamic equations using discretization methods and thus require a significant amount of time. As shown in Table 3, for the simulations of storm surge

inundation during Typhoon Lekima, the ADCIRC+SWAN coupled model taken 137843 s in CPU time while the HCA-FM model only taken 39.3 s. ~~The reduction in computational time as well as its high stability and universality would have great significance in the practical applications of storm surge inundation simulation.~~

Table 3: Grid type, resolution, number of cells and run time (CPU time) for the 1909 Lekima storm surge inundation simulations by HCA-FM and ADCIRC+SWAN model.

Model	Grid type	Resolution (m)	cells	Run CPU time (s)
ADCIRC+SWAN	triangle	100–1000	91290	137843
HCA-FM	rectangle	88 × 111	2301145	39.3

The reduction in computational time as well as its high stability and universality would have great significance in the practical applications of real-time early warning by rapidly identifying key affected areas on a large scale. HCA-FM can also leverage its computational efficiency to significantly reduce the time spent on probabilistic risk assessment that requires a large number of simulations, and contribute to more effective disaster prevention and mitigation strategies in coastal regions. As CA algorithms are well suited to parallel computation, it will be considered to apply parallel computation for HCA-FM model for further enhancement of computational efficiency in the future. Additional, consideration will also be given to designing an interactive operating system for the model to cater for more intuitive and easy use. In addition to improvement of efficiency, the principles of the model will also be improved in the future to take into account more comprehensive hydrodynamic mechanisms to improve the simulation accuracy.

5 Summary

In this paper, a novel storm surge inundation model (HCA-FM) based on a wetting and drying algorithm derived from the simplified shallow water momentum equation was proposed for quick and accurate simulation. The model triggered by boundary water level and flow velocity is built with an energy perspective considering the dominant impact factors including wind force and bottom friction. Moreover, the use of CA algorithm greatly improves the computational efficiency and computational stability. Credible comparison results to field observations for different regions and typhoon processes verified the model's accuracy in predicting the maximum flood extent and depth.

The HCA-FM reconciles computation cost and physical considerations when compared to other numerical and conceptual models. It is superior to traditional conceptual models in reflecting the hydrodynamic characteristics of storm surge inundation, and it also demonstrates its superiority over numerical models by significantly improving the computation efficiency. Therefore, the HCA-FM is a more appropriate candidate for predicting storm surge inundation in practical use.

Data availability

Experimental datasets in this paper are available at http://doi.org/10.5281/zenodo.10596631 (Gao et al., 2024). The HCA-FM codes and instruction file are available at http://doi.org/10.5281/zenodo.10596826 (Gao, 2024). Data sets including geographical, hydrological, and meteorological data that support ADCIRC+SWAN and HCA-FM model are publicly available, including the General Bathymetric Chart of the Oceans (GEBCO; https://www.gebco.net/), the ASTER GDEM V2 provided by Geospatial Data Cloud site, Computer Network Information Center, Chinese Academy of Sciences (http://www.gscloud.cn), the NCEP Climate Forecast System Reanalysis (CFSR, from 1979 to 2010, Saha et al., 2010; https://rda.ucar.edu/datasets/ds093.1/) and Version 2 (CFSv2, from 2010 to now, Saha et al., 2011; https://rda.ucar.edu/datasets/ds094.1/) Seclected Hourly Time-Series Products, and the GlobeLand30 land cover data openly available in National Geomatics Center of China (Chen et al, 2014; https://www.ngcc.cn/). The typhoon tracks are from the China Meteorological Administration tropical cyclone database (Ying et al., 2014, Lu et al., 2021; https://tcdata.typhoon.org.cn).

Author contributions

XG, SL, and PH contributed to model's conceptualization, methodology; XG contributed to code development and writing of manuscript draft; SL reviewed and edited the manuscript; DM and YL helped with the methodology.

Competing interests

The authors declare that they have no conflict of interest.

Acknowledgments

This research was sponsored by the National Key Research and Development Program of China (2023YFC3008200), the National Natural Science Foundation of China (42076214, 41976010, U1706216, U1806227).

We would like to acknowledge the ADCIRC+SWAN coupled model developed by the ADCIRC development team. We thanked the has data support provided by NCEP CFS, GEBCO, and CMA. We appreciated the technical support given by and the High Performance Computing Center, IOCAS and the data service provided by the Oceanographic Data Center, Chinese Academy of Sciences (CASODC) (http://msdc.qdio.ac.cn).

References

Akbar, M., Kanjanda, S., and Musinguzi, A.: Effect of Bottom Friction, Wind Drag Coefficient, and Meteorological Forcing in Hindcast of Hurricane Rita Storm Surge Using SWAN + ADCIRC Model, J. Mar. Sci. Eng., 5, 38, https://doi.org/10.3390/jmse5030038, 2017.

Bates, P. D., Dawson, R. J., Hall, J. W., Horritt, M. S., Nicholls, R. J., Wicks, J., and Mohamed Ahmed Ali Mohamed Hassan: Simplified two-dimensional numerical modelling of coastal flooding and example applications, Coast. Eng., 52, 793–810, https://doi.org/10.1016/j.coastaleng.2005.06.001, 2005.

Bates, P. D., Horritt, M. S., and Fewtrell, T. J.: A simple inertial formulation of the shallow water equations for efficient two-dimensional flood inundation modelling, J. Hydrol., 387, 33–45, https://doi.org/10.1016/j.jhydrol.2010.03.027, 2010.

Begmohammadi, A., Wirasaet, D., Silver, Z., Bolster, D., Kennedy, A. B., and Dietrich, J. C.: Subgrid surface connectivity for storm surge modeling, Adv. Water Resour., 153, 103939, https://doi.org/10.1016/j.advwatres.2021.103939, 2021.

Booij, N., Ris, R. C., and Holthuijsen, L. H.: A third-generation wave model for coastal regions: 1. Model description and validation, J. Geophys. Res. Oceans, 104, 7649–7666, https://doi.org/10.1029/98JC02622, 1999.

Bradbrook, K. F., Lane, S. N., Waller, S. G., and Bates, P. D.: Two dimensional diffusion wave modelling of flood inundation using a simplified channel representation, Int. J. River Basin Manag., 2, 211–223, https://doi.org/10.1080/15715124.2004.9635233, 2004.

Chen, A. S., Djordjevic, S., Leandro, J., and Savic, D.: The urban inundation model with bidirectional flow interaction between 2D overland surface and 1D sewer networks, Sixth International Conference on Sustainable Techniques and Strategies in Urban Water Management, Jun 2007, Lyon, France, https://hal.science/hal-03238883, 2007.

Chen, C., Beardsley, R. C., Luettich, R. A., Westerink, J. J., Wang, H., Perrie, W., Xu, Q., Donahue, A. S., Qi, J., Lin, H., Zhao, L., Kerr, P. C., Meng, Y., and Toulany, B.: Extratropical storm inundation testbed: Intermodel comparisons in Scituate, Massachusetts: EXTRATROPICAL STORM INUNDATION TESTBED, J. Geophys. Res. Oceans, 118, 5054–5073, https://doi.org/10.1002/jgrc.20397, 2013.

Chu, D., Zhang, J., Wu, Y., Jiao, X., and Qian, S.: Sensitivities of modelling storm surge to bottom friction, wind drag coefficient, and meteorological product in the East China Sea, Estuar. Coast. Shelf Sci., 231, 106460, https://doi.org/10.1016/j.ecss.2019.106460, 2019.

Dietrich, J. C., Zijlema, M., Westerink, J. J., Holthuijsen, L. H., Dawson, C., Luettich, R. A., Jensen, R. E., Smith, J. M., Stelling, G. S., and Stone, G. W.: Modeling hurricane waves and storm surge using integrally-coupled, scalable computations, Coast. Eng., 58, 45–65, https://doi.org/10.1016/j.coastaleng.2010.08.001, 2011.

Gao X.: HCA-FM code and instruction (Version v1), Zenodo [code], https://doi.org/10.5281/zenodo.10596826, 2024.

Gao, X., Li, S., Mo, D., Liu, Y., and Hu, P.: Data for HCA-FM Manuscript Submitted to GMD (Version v1), Zenodo [data set], https://doi.org/10.5281/zenodo.10596631, 2024.

Garratt, J. R.: Review of Drag Coefficients over Oceans and Continents, Mon. Weather Rev., 105, 915–929, https://doi.org/10.1175/1520-0493(1977)105<0915:RODCOO>2.0.CO;2, 1977.

GEBCO Bathymetric Compilation Group 2022: The GEBCO_2022 Grid - a continuous terrain model of the global oceans and land, NERC EDS British Oceanographic Data Centre NOC [data set], https://doi.org/10.5285/e0f0bb80-ab44-2739-e053-6c86abc0289c, 2022.

Hauer, M. E., Hardy, D., Kulp, S. A., Mueller, V., Wrathall, D. J., and Clark, P. U.: Assessing population exposure to coastal flooding due to sea level rise, Nature Communications, 12(1), 6900, https://doi.org/10.1038/s41467-021-27260-1, 2021.

Horritt, M. S. and Bates, P. D.: Effects of spatial resolution on a raster based model of flood flow, J. Hydrol., 253, 239–249, https://doi.org/10.1016/S0022-1694(01)00490-5, 2001.

Hunter, N. M., Bates, P. D., Horritt, M. S., and Wilson, M. D.: Simple spatially-distributed models for predicting flood inundation: A review, Geomorphology, 90, 208–225, https://doi.org/10.1016/j.geomorph.2006.10.021, 2007.

Jamali, B., Bach, P. M., Cunningham, L., and Deletic, A.: A Cellular Automata Fast Flood Evaluation (CA-fféé) Model, Water Resour. Res., 55, 4936–4953, https://doi.org/10.1029/2018WR023679, 2019.

Jamali, B., Löwe, R., Bach, P. M., Urich, C., Arnbjerg-Nielsen, K., and Deletic, A.: A rapid urban flood inundation and damage assessment model, J. Hydrol., 564, 1085–1098, https://doi.org/10.1016/j.jhydrol.2018.07.064, 2018.

Jun, C., Ban, Y., and Li, S.: Open access to Earth land-cover map, Nature, 514, 434–434, https://doi.org/10.1038/514434c, 2014.

Kalyanapu, A. J., Shankar, S., Pardyjak, E. R., Judi, D. R., and Burian, S. J.: Assessment of GPU computational enhancement to a 2D flood model, Environ. Modell. Softw., 26, 1009–1016, https://doi.org/10.1016/j.envsoft.2011.02.014, 2011.

Kennedy, A. B., Wirasaet, D., Begmohammadi, A., Sherman, T., Bolster, D., and Dietrich, J. C.: Subgrid theory for storm surge modeling, Ocean Model., 144, 101491, https://doi.org/10.1016/j.ocemod.2019.101491, 2019.

Li, Z., Li, S., Hou, Y., Mo, D., Li, J., and Yin, B.: Typhoon-induced wind waves in the northern East China Sea during two typhoon events: the impact of wind field and wave-current interaction, J. Ocean. Limnol., 40, 934–949, https://doi.org/10.1007/s00343-021-1089-7, 2022.

Li, Z., Li, S., Hu, P., Feng, X., Mo, D., and Li, J.: Improving storm surge simulations by considering wave-steepness-dependent drag coefficient in the northern East China Sea, Ocean Model., 186, 102283, https://doi.org/10.1016/j.ocemod.2023.102283, 2023.

Liu, Z., Merwade, V., and Jafarzadegan, K.: Investigating the role of model structure and surface roughness in generating flood inundation extents using one- and two-dimensional hydraulic models, J. Flood Risk Manag., 12, e12347, https://doi.org/10.1111/jfr3.12347, 2019.

Lu, X., Yu, H., Ying, M., Zhao, B., Zhang, S., Lin, L., Bai, L., and Wan, R.: Western North Pacific Tropical Cyclone Database Created by the China Meteorological Administration, Adv. Atmos. Sci., 38, 690–699, https://doi.org/10.1007/s00376-020-0211-7, 2021.

Luettich, R. A. and Westerink, J. J.: Elemental Wetting and Drying in the ADCIRC Hydrodynamic Model: Upgrades and Documentation for ADCIRC Version 34.XX, Contractors Report, Department of the Army, US Army Corps of Engineers, Waterways Experiment Station, Vicksburg, MS., March 1999, 8 p., https://adcirc.org/wp-content/uploads/sites/2255/2018/11/1999_Luettich01.pdf, 1999.

Luettich, R. A., Westerink, J. J., and Scheffner N. W.: ADCIRC: an advanced three-dimensional circulation model for shelves coasts and estuaries, report 1: theory and methodology of ADCIRC-2DDI and ADCIRC-3DL, Dredging Research Program Technical Report DRP-92-6, U.S. Army Engineers Waterways Experiment Station, Vicksburg, MS, 137p., https://adcirc.org/wp-content/uploads/sites/2255/2018/11/1992_Luettich02.pdf, 1992.

Machineni, N., Sinha, V. S. P., Singh, P., and Reddy, N. T.: The impact of distributed landuse information in hydrodynamic model application in storm surge inundation, Estuar. Coast. Shelf Sci., 231, 106466, https://doi.org/10.1016/j.ecss.2019.106466, 2019.

Manfreda, S. and Samela, C.: A digital elevation model based method for a rapid estimation of flood inundation depth, J. Flood Risk Manag., 12, e12541, https://doi.org/10.1111/jfr3.12541, 2019.

Mao, M. and Xia, M.: Dynamics of wave–current–surge interactions in Lake Michigan: A model comparison, Ocean Model., 110, 1–20, https://doi.org/10.1016/j.ocemod.2016.12.007, 2017.

Medeiros, S. C. and Hagen, S. C.: Review of wetting and drying algorithms for numerical tidal flow models: REVIEW OF WETTING AND DRYING ALGORITHMS FOR NUMERICAL TIDAL FLOW MODELS, Int. J. Numer. Meth. Fluids, 71, 473–487, https://doi.org/10.1002/fld.3668, 2013.

Miura, Y., Mandli, K. T., and Deodatis, G.: High-Speed GIS-Based Simulation of Storm Surge–Induced Flooding Accounting for Sea Level Rise, Nat. Hazards Rev., 22, 04021018, https://doi.org/10.1061/(ASCE)NH.1527-6996.0000465, 2021.

Nakamura, R., Mäll, M., and Shibayama, T.: Street-scale storm surge load impact assessment using fine-resolution numerical modelling: a case study from Nemuro, Japan, Nat. Hazards, 99, 391–422, https://doi.org/10.1007/s11069-019-03746-6, 2019.

Parizi, E., Khojeh, S., Hosseini, S. M., and Moghadam, Y. J.: Application of Unmanned Aerial Vehicle DEM in flood modeling and comparison with global DEMs: Case study of Atrak River Basin, Iran, J. Environ. Manage., 317, 115492, https://doi.org/10.1016/j.jenvman.2022.115492, 2022.

Roberts, K. J., Casey Dietrich, J., Wirasaet, D., Pringle, W. J., and Westerink, J. J.: Dynamic load balancing for predictions of storm surge and coastal flooding, Environ. Modell. Softw., 140, 105045, https://doi.org/10.1016/j.envsoft.2021.105045, 2021.

Saha, S., Moorthi, S., Pan, H., Wu, X., Wang, J., Nadiga, S., Tripp, P., Kistler, R., Woollen, J., Behringer, D., Liu, H., Stokes, D., Grumbine, R., Gayno, G., Wang, J., Hou, Y., Chuang, H., Juang, H. H., Sela, J., Iredell, M., Treadon, R., Kleist, D., Delst, P. V., Keyser, D., Derber, J., Ek, M., Meng, J., Wei, H., Yang, R., Lord, S., van den Dool, H., Kumar, A., Wang, W., Long, C., Chelliah, M., Xue, Y., Huang, B., Schemm, J., Ebisuzaki, W., Lin, R., Xie, P., Chen, M., Zhou, S., Higgins,

W., Zou, C., Liu, Q., Chen, Y., Han, Y., Cucurull, L., Reynolds, R. W., Rutledge, G., and Goldberg, M.: NCEP Climate Forecast System Reanalysis (CFSR) Selected Hourly Time-Series Products, January 1979 to December 2010, Research Data Archive at the National Center for Atmospheric Research, Computational and Information Systems Laboratory [data set], https://doi.org/10.5065/D6513W89, 2010.

Saha, S., Moorthi, S., Wu, X., Wang, J., Nadiga, S., Tripp, P., Behringer, D., Hou, Y., Chuang, H., Iredell, M., Ek, M., Meng, J., Yang, R., Mendez, M. P., van den Dool, H., Zhang, Q., Wang, W., Chen, M., and Becker, E.: NCEP Climate Forecast System Version 2 (CFSv2) Selected Hourly Time-Series Products, Research Data Archive at the National Center for Atmospheric Research, Computational and Information Systems Laboratory [data set], https://doi.org/10.5065/D6N877VB, 2011.

Sanders, B. F., Schubert, J. E., and Detwiler, R. L.: ParBreZo: A parallel, unstructured grid, Godunov-type, shallow-water code for high-resolution flood inundation modeling at the regional scale, Adv. Water Resour., 33, 1456–1467, https://doi.org/10.1016/j.advwatres.2010.07.007, 2010.

Saswati Deb, Huijie Xue, and Shivanesh Rao: Saco-Casco Bays Inundation Modeling of Five Winter Storms, Journal of Shipping and Ocean Engineering, 11, https://doi.org/10.17265/2159-5879/2021.02.001, 2021.

Sehili, A., Lang, G., and Lippert, C.: High-resolution subgrid models: background, grid generation, and implementation, Ocean Dyn., 64, 519–535, https://doi.org/10.1007/s10236-014-0693-x, 2014.

Shi, S., Yang, B., and Jiang, W.: Numerical simulations of compound flooding caused by storm surge and heavy rain with the presence of urban drainage system, coastal dam and tide gates: A case study of Xiangshan, China, Coast. Eng., 172, 104064, https://doi.org/10.1016/j.coastaleng.2021.104064, 2022.

Teng, J., Jakeman, A. J., Vaze, J., Croke, B. F. W., Dutta, D., and Kim, S.: Flood inundation modelling: A review of methods, recent advances and uncertainty analysis, Environ. Modell. Softw., 90, 201–216, https://doi.org/10.1016/j.envsoft.2017.01.006, 2017.

Tsubaki, R. and Kawahara, Y.: The uncertainty of local flow parameters during inundation flow over complex topographies with elevation errors, J. Hydrol., 486, 71–87, https://doi.org/10.1016/j.jhydrol.2013.01.042, 2013.

Vacondio, R., Dal Palù, A., Ferrari, A., Mignosa, P., Aureli, F., and Dazzi, S.: A non-uniform efficient grid type for GPU-parallel Shallow Water Equations models, Environ. Modell. Softw., 88, 119–137, https://doi.org/10.1016/j.envsoft.2016.11.012, 2017.

Volp, N. D., Van Prooijen, B. C., and Stelling, G. S.: A finite volume approach for shallow water flow accounting for high-resolution bathymetry and roughness data: Subgrid-Based Finite Volume Method, Water Resour. Res., 49, 4126–4135, https://doi.org/10.1002/wrcr.20324, 2013.

Wang, K., Hou, Y., Li, S., Du, M., and Li, R.: Numerical Study of Storm Surge Inundation in the Southwestern Hangzhou Bay Region During Typhoon Chan-Hom in 2015, J. Ocean Univ. China, 19, 263–271, https://doi.org/10.1007/s11802-020-4258-y, 2020.

Wang, N., Hou, Y., Mo, D., and Li, J.: Hazard assessment of storm surges and concomitant waves in Shandong Peninsula based on long-term numerical simulations, Ocean Coastal Manage., 213, 105888, https://doi.org/10.1016/j.ocecoaman.2021.105888, 2021.

Westerink, J. J., Blain C. A., Luettich R. A., and Scheffner N. W.: ADCIRC: an advanced three-dimensional circulation model for shelves coasts and estuaries, report 2: users manual for ADCIRC-2DDI, Dredging Research Program Technical Report DRP-92-6, U.S. Army Engineers Waterways Experiment Station, Vicksburg, MS., 156p., https://adcirc.org/wp-content/uploads/sites/2255/2018/11/1994_Westerink01.pdf, 1994.

Wijaya, O. T. and Yang, T. H.: A Novel Hybrid Approach Based on Cellular Automata and a Digital Elevation Model for Rapid Flood Assessment, Water, 13, 1311, https://doi.org/10.3390/w13091311, 2021.

Wijaya, O. T. and Yang, T. H.: Combining two algorithms as a transition rules for CA-based inundation model. In Proceedings of the 22nd IAHR APD, Saporo, Japan, 15–16 September 2020, https://www.researchgate.net/publication/343850058, 2020.

Wolfram, S.: Cellular automata as models of complexity, Nature, 311, 419–424, https://doi.org/10.1038/311419a0, 1984.

Woodruff, J. L., Dietrich, J. C., Wirasaet, D., Kennedy, A. B., Bolster, D., Silver, Z., Medlin, S. D., and Kolar, R. L.: Subgrid corrections in finite-element modeling of storm-driven coastal flooding, Ocean Model., 167, 101887, https://doi.org/10.1016/j.ocemod.2021.101887, 2021.

Ying, M., Zhang, W., Yu, H., Lu, X., Feng, J., Fan, Y., Zhu, Y., and Chen, D.: An Overview of the China Meteorological Administration Tropical Cyclone Database, J. Atmos. Ocean. Technol., 31, 287–301, https://doi.org/10.1175/JTECH-D-12-00119.1, 2014.